
Proceedings Paper:
Zhu, Y., Kang, L. and Zhang, L.X. orcid.org/0000-0002-4535-3200 (Accepted: 2025) Impact of 5G Network Slicing on Efficiency and Stability Control of Base Station Microgrids. In: Proceedings of 2025 IEEE Conference on Antenna Measurements and Applications. 2025 IEEE Conference on Antenna Measurements and Applications, 18-20 Nov 2025, Antibes, France. IEEE. (In Press)

Impact of 5G Network Slicing on Efficiency and Stability Control of Base Station Microgrids

Yingqi Zhu
School of Electronic and Electrical Engineering
University of Leeds
Leeds, United Kingdom
elyzhu@leeds.ac.uk

Kang Li
School of Electronic and Electrical Engineering
University of Leeds
Leeds, United Kingdom
k.li1@leeds.ac.uk

Li Zhang
School of Electronic and Electrical Engineering
University of Leeds
Leeds, United Kingdom
l.x.zhang@leeds.ac.uk

***Abstract*—As power systems with multiple microgrids evolve to integrate distributed and renewable energy sources across different areas and regions, maintaining stable microgrid voltage and frequency control becomes increasingly reliant on fast and reliable communication infrastructure. Despite recent progress in wireless communication, many existing solutions still suffer from latency and packet loss that degrade control loop performance. This work presents a simulation framework that couple DC microgrids with proportional–integral (PI) voltage control loops and a 5G slicing-aware wireless communication model. A Q-learning-based algorithm is introduced to dynamically allocate bandwidth between two microgrids across three network slice types, namely legacy, shared, and ultra-reliable low-latency communication (URLLC) to optimize control performance under constrained radio resources. The impact of communication latency and reliability is evaluated through key performance indicators including voltage recovery, control reward, delay, packet loss, and throughput. Simulation results demonstrate that URLLC slicing significantly enhances control performance. Specifically, it reduces voltage recovery time by approximately 24%, lowers control-packet loss rate by up to 70% relative to legacy modes, and sustains a throughput improvement exceeding 20%. These results underscore the pivotal role of low-latency and high-reliability communication in enabling stable and efficient smart grid operation.**

***Index Terms*—5G, network slicing, URLLC, microgrids, voltage control.**

I. Introduction

As modern power systems with multiple microgrids embedded across different areas and regions are evolving into cyber-physical systems, communication networks play a critical role in enabling distributed sensing, coordination, and control [1], [2]. However, most existing microgrid deployments rely on power line communication (PLC), or Wi-Fi, all of which lack the ultra-low latency and high reliability required for fast control loops. While fifth-generation (5G) networks, particularly ultra-reliable low-latency communication (URLLC), offer promising capabilities, their integration into microgrid simulation and control design remains limited [3]–[5]. In particular, the impact of slice-level quality of service (QoS) characteristics, such as communication delay and packet loss, on control loop performance is rarely examined in existing microgrid studies. This highlights a critical gap in modeling the co-effects of advanced wireless communication features and power system control dynamics, especially under heterogeneous slicing conditions.

Most existing works on 5G slicing emphasize communication-side performance, with limited attention to how slicing affects real-time control in power systems. Zhou et al. [6] proposed a deep transfer reinforcement learning (DTRL) scheme for joint radio and cache resource allocation to serve 5G radio access network (RAN) slicing, but their work primarily focuses on algorithmic optimization within the communication layer. Choudhury et al. [7] developed a coordinated set-point automatic adjustment with correction enabled (C-SPAACE) framework for microgrid control using 5G slicing and introduced an age of information (AoI)-based scheduler for spectrum allocation. While it emphasizes communication-aware coordination, it primarily addresses resource scheduling without considering the impact of slice-specific QoS on the control performance. Feng et al. [8] leveraged 5G RAN slicing to optimize virtual power plant (VPP) scheduling for economic gains, whereas this paper focuses on how slicing-induced communication dynamics impact closed-loop control performance in microgrids. Troia et al. [9] optimized 5G slice admission using deep reinforcement learning, focusing on network-level resource allocation without addressing control-layer performance. Meng et al. [10] proposed a DRL-based strategy for smart grid RAN slice allocation, emphasizing adaptive bandwidth management for elastic and real-time applications. However, their work focused solely on network-level resource optimization, without analyzing the impact on microgrid control performance such as voltage regulation.

In this paper, we propose a simulation framework that integrates simplified DC microgrid models with PI-based voltage control loops and a 5G RAN slicing-aware communication network. A Q-learning-based algorithm is employed to dynamically allocate bandwidth between microgrids under different slicing modes. The framework explicitly models communication-induced latency and packet loss to evaluate their impact on system performance. Simulation results demonstrate that slice-specific QoS has a significant influence on voltage recovery and control efficiency, as reflected by re-

ward evolution, delay profiles, packet loss rates, and throughput trends. These findings provide insights for the co-design of wireless communication and power control strategies in intelligent energy systems.

II. System Model and Problem Formulation

A. Microgrid Topology and Control Model

Fig. 1 illustrates the overall system configuration, featuring base station microgrids (BSMG1 and BSMG2) equipped with photovoltaic (PV), wind generation, energy storage, and centralized energy management systems. Both microgrids communicate via a 5G network infrastructure that provides three types of RAN slices. These slices differ in their latency and reliability characteristics and are used to transmit the control signals from the centralized voltage controller.

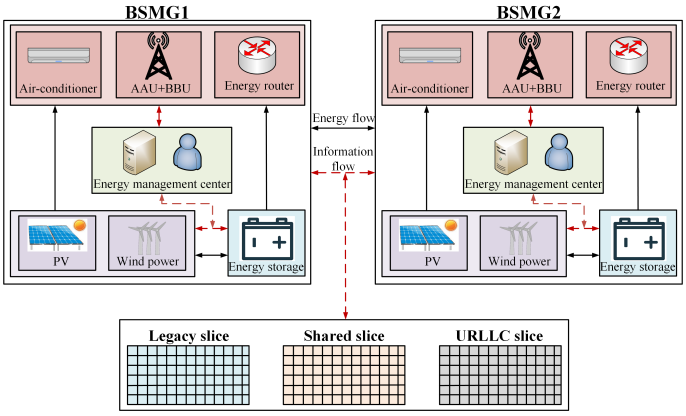

Fig. 1. RAN slices model for BSMG

To evaluate the impact of communication impairments on voltage regulation, we build a simplified DC microgrid model consisting of two battery-inverter units connected to a common DC bus that supplies a constant-power load. For simplicity, the following assumptions are adopted:

1) **Single-bus topology:** All generation and load are connected to one node, enabling centralized control analysis.
2) **Constant-power load:** The load steps from 1 kW to 2 kW at $t = 0.1$ s, creating a voltage disturbance to evaluate the controller's transient response.
3) **Lumped bus capacitance:** All DC bus and inverter filter capacitors are aggregated into an equivalent capacitance C_{eq}.

The goal of the PI controller is to regulate the DC-bus voltage $V_{\text{bus}}(k)$ to match a predefined reference value V_{ref}.

- **Error calculation**

$$e(k) = V_{\text{ref}} - V_{\text{bus}}(k) \tag{1}$$

where $e(k)$ is the voltage error at step k.

- **Proportional and integral Terms**

$$u_{\text{unsat}}(k) = K_p e(k) + K_i \sum_{i=0}^{k} e(i)\Delta t \tag{2}$$

where $u_{\text{unsat}}(k)$ is the final control signal before saturation, K_p is proportional gain, and K_i is integral gain.

- **Limiting and final control current**

$$I_{\text{batt}}(k) = \text{sat}\big(u_{\text{unsat}}(k), I_{\min}, I_{\max}\big) \tag{3}$$

where sat() is a saturation function, $I_{\text{batt}}(k)$ denotes the instantaneous battery output current delivered to the DC bus at time step k, and $I_{\min}$ and $I_{\max}$ represent saturation limits.

B. Bus Voltage Dynamics

According to the relationship between capacitor charging and discharging, the bus voltage update formula is shown as:

$$C_{eq}\frac{dV_{\text{bus}}(k)}{dt} = I_{\text{batt}}(k) - I_{\text{load}}(k) \tag{4}$$

where $I_{\text{load}}(k)$ is the current drawn by the load.

The discrete-time form after transformation is:

$$V_{\text{bus}}(k+1) = V_{\text{bus}}(k) + \big(I_{\text{batt}}(k) - I_{\text{load}}(k)\big)\frac{\Delta t}{C_{eq}} \tag{5}$$

where k is discrete time index, $P_{\text{load}}(k)$ is constant power load at time step k, Δt is the simulation time step.

C. 5G RAN Slicing Model

To accurately describe the transmission characteristics of microgrid control commands under 5G RAN slicing, we model each wireless link as a superposition of Rayleigh small-scale fading and constant additive white Gaussian noise (AWGN).

- **Rayleigh fading**

The complex channel gain $h(k)$ at time step k is modeled as a zero-mean and circularly symmetric complex Gaussian random variable:

$$h(k) \sim \mathcal{CN}(0, \sigma_r^2) \tag{6}$$

where σ_r^2 is the variance of the underlying Gaussian process.

Consequently, the instantaneous power gain $|h(k)|^2$ follows an exponential distribution:

$$f_{|h|^2}(x) = \frac{1}{\sigma_r^2}\exp\left(-\frac{x}{\sigma_r^2}\right), \quad x \geq 0 \tag{7}$$

where x is the realized power gain, and $f_{|h|^2}(x)$ is the probability density function.

- **AWGN noise power**

The receiver observes additive white Gaussian noise with constant power:

$$N_0 = \sigma_g \tag{8}$$

where N_0 is the one-sided noise power spectral density, and σ_g is the variance of the AWGN.

- **Signal-to-Noise Ratio (SNR)**

With normalized transmit power P_{tx}, the SNR is:

$$\text{SNR}(k) = \frac{P_{\text{tx}} |h(k)|^2}{N_0} \tag{9}$$

- **Spectral efficiency and capacity**

Under the Shannon capacity formula, the spectral efficiency is:

$$\eta(k) = \log_2 (1 + \text{SNR}(k)) \tag{10}$$

where $\eta(k)$ is spectral efficiency at time k.

The instantaneous link capacity is:

$$C_k = b\,\eta(k) \tag{11}$$

where C_k is instantaneous capacity, and b is allocated bandwidth.

- **Packet transmission delay**

For a control packet of size B bits, the one-way transmission delay is:

$$d(k) = \frac{B}{C(k)} \tag{12}$$

where $d(k)$ is transmission delay at time k.

- **Packet loss probability**

A packet is considered lost if either the transmission delay exceeds a slice-specific threshold or a random radio resource loss occurs due to insufficient bandwidth. The overall loss probability is:

$$P_{\text{loss}}(k) = 1-(1 - 1\{\text{Delay}(k) > D_{\text{th}}\}) (1 - p_{\text{radio}}(b)) \tag{13}$$

where $P_{\text{loss}}(k)$ is total loss probability at time k, $1\{\}$ is the indicator function (1 if condition true, else 0), D_{th} is slice-specific maximum acceptable delay, and $p_{\text{radio}}(b)$ is baseline radio loss probability.

III. Deep Reinforcement Learning-Based Slicing Algorithm

To dynamically allocate RAN slice bandwidth between two BSMGs, we cast the problem as a Markov decision process and employ a Q-learning agent. At each discrete time step k, the agent observes a system state s_k, selects an action a_k, receives an immediate reward r_k, and updates its action-value function $Q(s, a)$.

A. State Representation

The state vector captures both overall voltage regulation error and inter-microgrid voltage imbalance:

$$s_k = (e_{\text{avg}}(k),\, v_{\text{diff}}(k)) \tag{14}$$

$$e_{\text{avg}}(k) = V_{\text{ref}} - \frac{1}{2} (V_1(k) + V_2(k)) \tag{15}$$

$$v_{\text{diff}} = |V_1(k) - V_2(k)| \tag{16}$$

where $V_i(k)$ is the measured voltage of microgrid i at time k, $e_{\text{avg}}(k)$ denotes the average voltage regulation error, and $v_{\text{diff}}(k)$ represents the voltage imbalance between the two microgrids.

B. Action Space

At each instant, the RL agent chooses how much of the total bandwidth pool to allocate to BSMG1, and then BSMG2 automatically receives what remains.

$$b = b_1(k) + b_2(k) \tag{17}$$

where $b_1(k)$ and $b_2(k)$ are bandwidth assigned to BSMG1 and BSMG2 at time k, respectively.

C. Reward Function

The instantaneous reward is designed to evaluate both communication performance and control stability. It is expressed as a weighted combination of spectral efficiency, utility, and penalty terms:

$$\begin{aligned} r_k = {} & \lambda\big[\eta_1(k) + \eta_2(k)\big] + \mu U_e(k) + \xi U_\pi(k) \\ & - \alpha\big[d_1(k) + d_2(k)\big] - \beta\big[p_{\text{loss},1}(k) + p_{\text{loss},2}(k)\big] \\ & - \gamma v_{\text{diff}}(k) \end{aligned} \tag{18}$$

$$U_e(k) = 1 - \exp\left(-k_0 \frac{b}{b_{\max}}\right) \tag{19}$$

$$U_\pi(k) = 1 - \exp\left(-k_1 \frac{b^2}{k_2 + b}\right) \tag{20}$$

where $\eta_i(k)$ is spectral efficiency of BSMG i at time k, $U_e(k)$ is utility of elastic slice, $U_\pi(k)$ is utility of real-time slice, $d_i(k)$ is packet delay for BSMG i, $p_{\text{loss},i}(k)$ is loss probability for MG i. $\lambda, \mu, \xi, \alpha, \beta, \gamma$ are weights to balance system objectives, and k_0, k_1, and k_2 are slice utility shaping parameters.

D. Q-Learning Update

To optimize the bandwidth allocation strategy, we employ the classical Q-learning algorithm. The agent maintains an action-value function, which estimates the expected cumulative reward of taking action a_k in state s_k. After executing action a_k, receiving reward r_k, and transitioning to the next state s_{k+1}, the Q-value is updated as follows:

$$Q(s_k, a_k) \leftarrow Q(s_k, a_k) + \alpha_Q \big[r_k + \gamma_D \max_{a'} Q(s_{k+1}, a') - Q(s_k, a_k) \big] \tag{21}$$

where α_Q is the learning rate, which controls how much newly acquired information overrides the old, γ_D is the discount factor, representing the importance of future rewards, and $\max Q(s_{k+1}, a')$ reflects the Bellman optimality principle, estimating the value of the best future action at the next state.

To balance exploration and exploitation, the agent follows an ε-greedy policy. Specifically, with probability $\varepsilon \leq 1$, a random action is selected to promote exploration. Otherwise, the action with the highest estimated Q-value is chosen.

IV. Simulation Results

A. Simulation Setup

To evaluate the proposed joint control and slicing strategy, we simulate a two BSMGs system connected to a common DC bus, as previously described. Each BSMG consists of an inverter-based generator and serves one of the three network slice types: legacy, shared, and URLLC. The system is subjected to a step load change from 1 kW to 2 kW at 0.1 s, inducing a voltage transient to test the dynamic performance of the voltage regulation.

The simulation is implemented in MATLAB with a time step of $\Delta t = 0.1$ ms. Each simulation lasts 300 ms. The nominal bus voltage is set to $V_{\text{ref}} = 380$ V, and the equivalent bus-side capacitance is $C_{\text{eq}} = 50$ µF. The load disturbance occurs at 100 ms, and all inverter controllers adopt the same PI control parameters for consistency across different slices.

In the communication layer, bandwidth allocation is discretized into 0–8 MHz. For each MG, the control packet is 80 bits long, and delay is computed using the Shannon capacity model with Rayleigh fading and AWGN channel assumptions. The Q-learning agent dynamically adjusts the bandwidth of each slice to optimize a reward function that jointly considers throughput, delay, packet loss, and voltage deviation penalties.

B. Results Analysis

Fig. 2 shows the DC bus voltage recovery following a load disturbance at 100 ms. All configurations exhibit prompt voltage regulation, but differences arise across microgrids and slice types. Among the slicing schemes, URLLC achieves the quickest voltage restoration, with recovery times around 160 ms, compared to 190 ms for the shared slice and 210 ms for the legacy slice, representing a 24% reduction in recovery time relative to the legacy configuration. This improvement highlights the benefit of low-latency communication in enhancing transient control responsiveness. Shared slices offer intermediate performance, while legacy slices recover more slowly and exhibit larger voltage deviations. These results confirm the effectiveness of latency-aware slicing in improving voltage stability under load transients.

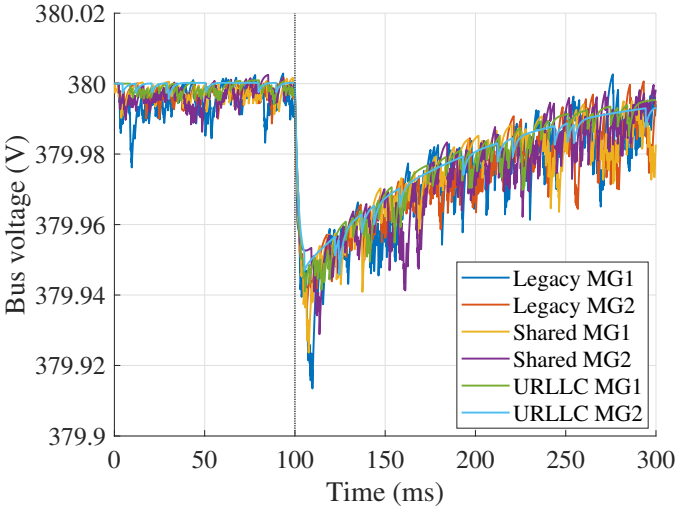

Fig. 2. Bus voltage recovery

Fig. 3 presents the reward evolution of different slice types in BSMG1. The URLLC slice consistently achieves the highest average reward, stabilizing around 1.0, benefiting from its prioritized access to bandwidth and strict delay constraints. In contrast, the shared and legacy slices achieve lower average rewards of approximately 0.6 and 0.4, respectively, and exhibit greater temporal fluctuation due to their lower or adaptive priority in bandwidth allocation. These results validate the reward function's ability to capture service differentiation and highlight the advantage of URLLC in maintaining consistent control performance.

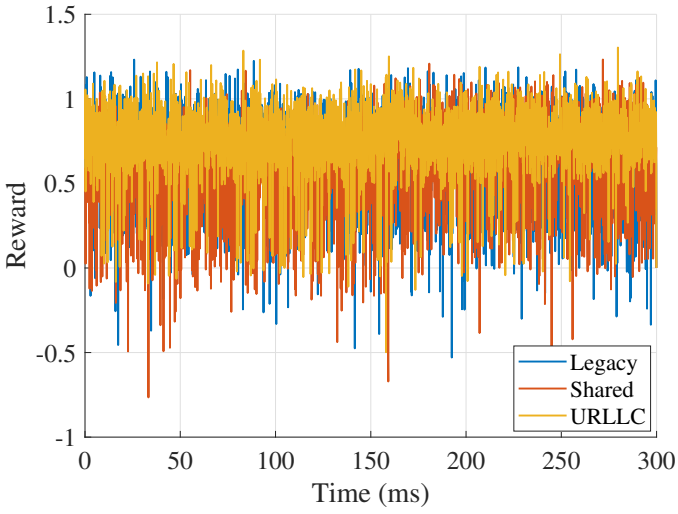

Fig. 3. Reward

Fig. 4 shows the distribution of control packet transmission delays across different slice types and microgrids. It is evident that the majority of URLLC packets experience delays below 3 ms, with over 80% concentrated in the first three bins (0–3 ms), reflecting the effectiveness of latency-aware allocation. In contrast, legacy slices exhibit a wider delay spread, with a significant number of packets experiencing delays exceeding 10 ms. Shared slices fall in between, with moderate dispersion and a peak around 5–7 ms. These results confirm that the proposed slicing mechanism successfully prioritizes URLLC traffic while maintaining acceptable delay for other service types.

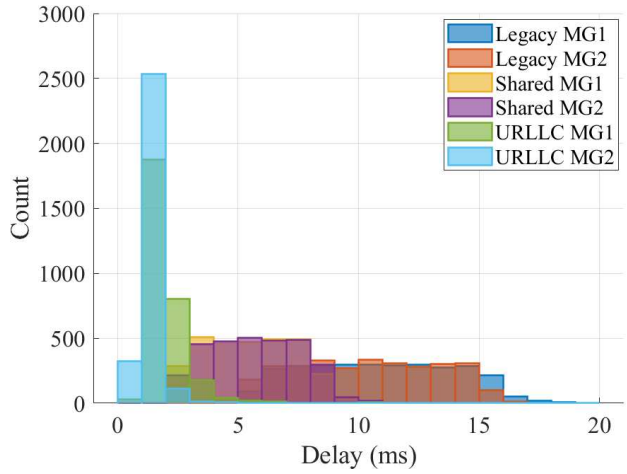

Fig. 4. Latency distribution

Fig. 5 presents the cumulative packet loss rate for each slice type. The URLLC slices exhibit the lowest loss rate, stabilizing below 4% throughout the simulation, which is approximately 70% lower than the legacy slices in BSMG1, whose loss rate converges around 13.5%. Shared slices maintain moderate performance, with loss rates settling between 6–10%.

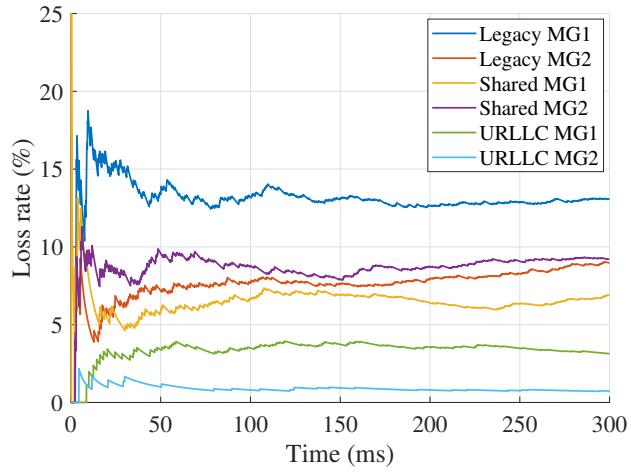

Fig. 5. Packet loss rate

Fig. 6 illustrates the slice-wise throughput dynamics over time, calculated using a 50 ms moving average window. After an initial convergence period within the first 100 ms, the throughput stabilizes across all configurations. URLLC slices consistently achieve the highest throughput, reaching approximately 20 pkt/s, which is 15–20% higher than the shared slices (17.5 pkt/s) and 25–30% higher than the legacy slices (16 pkt/s). This performance gain is attributed to URLLC's prioritized access to spectrum resources and its latency-aware scheduling mechanism. The results underscore the system's ability to ensure differentiated service levels and highlight the throughput-efficiency advantage of URLLC under the proposed resource allocation policy.

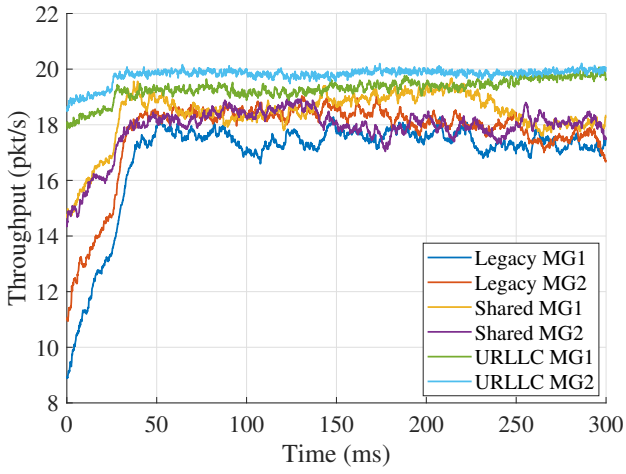

Fig. 6. Throughput

Table I summarizes the performance metrics of different slice types in BSMG1 based on the simulation results shown in Fig. 2–Fig. 6.

TABLE I
PERFORMANCE COMPARISON OF SLICE TYPES IN BSMG1

Metric	URLLC	Shared	Legacy
Voltage recovery time (ms)	160	190	210
Average reward	1.0	0.6	0.4
Delay (ms)	0–3	5–7	> 10
Packet loss rate (%)	4	6	13.5
Throughput (pkt/s)	20	17.5	16

V. CONCLUSION

This work presents a simulation framework integrating microgrid control and 5G communication, enabling joint evaluation of control performance under varying communication qualities. The framework models DC microgrids with distributed inverter-based units regulated by PI controllers, where control packets are delivered via emulated 5G network slices. The analysis of voltage regulation, bandwidth allocation, and communication metrics reveals several key findings, summarized as follows:

1) Communication quality directly influences voltage regulation performance. Following the load disturbance

at 100 ms, all slices restore bus voltage, but URLLC achieves the fastest recovery. Compared to the legacy slice, URLLC shortens the settling time by 24%, demonstrating improved responsiveness under low-latency conditions.

2) The slicing-aware strategy enables dynamic and priority-driven resource allocation. During transients, bandwidth is adaptively allocated, with URLLC receiving the largest share to ensure timely control. Consequently, URLLC achieves the highest average reward (1.0), outperforming shared (0.6) and legacy (0.4) slices, validating both reward design and slice prioritization.
3) Slicing enhances communication reliability and reduces delay. Over 95% of URLLC packets are delivered within 5 ms, while legacy traffic shows delays up to 20 ms. Packet loss for URLLC remains below 4%, approximately 70% lower than the 13% observed in legacy slices, highlighting the value of differentiated QoS in latency-sensitive control.
4) URLLC slicing improves throughput and scalability. URLLC sustains the highest throughput (20 pkt/s), exceeding shared (17.5 pkt/s) and legacy (16 pkt/s) modes. This demonstrates its advantage in supporting dense control traffic while maintaining low-latency performance.

Overall, this study highlights the necessity of joint control-communication design in future microgrids and showcases how network slicing, particularly URLLC, can significantly enhance the resilience and performance of cyber-physical energy systems.

REFERENCES

[1] A. J. Taveras Cruz, M. Aybar-Mejía, Y. Díaz Roque, K. Coste Ramírez, J. G. Durán, D. Rosario Weeks, D. Mariano-Hernández, and L. Hernández-Callejo, "Implications of 5G technology in the management of power microgrids: a review of the literature," *Energies*, vol. 16, no. 4, pp. 1–13, Feb. 2023.

[2] T. Srinivasan, S. Venkatapathy, H. G. Jo, and I. H. Ra, "VNF-enabled 5G network orchestration framework for slice creation, isolation and management," *J. Sens. Actuator Netw.*, vol. 12, no. 5, pp. 65, Sep. 2023.

[3] J. Wallace, M. Vukovic, T. Karimovic, and W. Edwards, "A high-performance 5G/6G framework for smart cities supporting multi-level artificial intelligence," in *Proc. 2025 2nd Int. Conf. on Advanced Innovations in Smart Cities (ICAISC)*, pp. 1–9, Feb. 2025.

[4] X. Zhou, Z. Li, X. Liu, and Z. Zhou, "Latest research progress and practice of 5G slicing technology in China's new power system," in *Proc. 2023 8th Asia Conf. on Power and Electrical Engineering (ACPPEE)*, pp. 1509–1516, Apr. 2023.

[5] S. S. Sefati and S. Halunga, "Ultra-reliability and low-latency communications on the internet of things based on 5G network: literature review, classification, and future research view," *Trans. Emerg. Telecommun. Technol.*, vol. 34, no. 6, pp. e4770, Jun. 2023.

[6] H. Zhou, M. Erol-Kantarci, and H. V. Poor, "Learning from peers: Deep transfer reinforcement learning for joint radio and cache resource allocation in 5G RAN slicing," *IEEE Trans. Cogn. Commun. Netw.*, vol. 8, no. 4, pp. 1925–1941, Dec. 2022.

[7] B. Choudhury, A. Mohammadhassani, B. Alexander, R. Iyer, A. Mehrizi-Sani, J. H. Reed, and V. K. Shah, "Control coordination in inverter-based microgrids using AoI-based 5G schedulers," *IET Smart Grid*, vol. 7, no. 1, pp. 38–50, Feb. 2024.

[8] C. Feng, Q. Chen, Y. Wang, J. Ma, and X. Wang, "Frequency regulation service provision for virtual power plants through 5G RAN slicing," *IEEE Trans. Smart Grid*, vol. 13, no. 6, pp. 4943–4956, Nov. 2022.

[9] S. Troia, A. F. R. Vanegas, L. M. M. Zorello, and G. Maier, "Admission control and virtual network embedding in 5G networks: A deep reinforcement-learning approach," *IEEE Access*, vol. 10, pp. 15860–15875, Feb. 2022.

[10] S. Meng, Z. H. Wang, H. X. Ding, S. Wu, X. Li, P. Zhao, C. Y. Zhu, and X. Wang, "RAN slice strategy based on deep reinforcement learning for smart grid," in *Proc. 2019 Computing, Communications and IoT Applications (ComComAp)*, pp. 6–11, Oct. 2019.